EUROPEAN ORGANIZATION FOR NUCLEAR RESEARCH

Proposal to the ISOLDE and Neutron Time-of-Flight Committee

Probing the local environments and optical properties in halide perovskites with short-lived radioactive isotopes

January 10, 2024

H. Masenda[1], J. Borchert[2,3], D. Naidoo[1], K. Jakata[4], K. Johnston[5], K. Bharuth-Ram[6,7], H. P. Gunnlaugsson[8], O. Er-Raji[2,3], Y. Gupta[2,3], R. Mantovan[9], O. Mpatani[1], L.I. Lisema[1], S.G. Dlamini [7]J. Schell[5,10], A. Mokhles Gerami[5,12] and The Mössbauer Collaboration at ISOLDE/CERN[4].

[1]*School of Physics, University of the Witwatersrand, Johannesburg, 2050, South Africa*, [2]*Division Photovoltaics (PV), Fraunhofer Institute for Solar Energy Systems ISE, Heidenhofstr. 2, 79110 Freiburg, Germany*, [3]*Department of Sustainable Systems Engineering (INATECH), University of Freiburg, Emmy-Noether-Str. 2, 79110 Freiburg, Germany*, [4]*Diamond Light Source Ltd, Oxfordshire, OX11 0DE, England*, [5]*PH Dept, ISOLDE/CERN, 1211 Geneva 23, Switzerland*, [6]*School of Chemistry and Physics, University of KwaZulu-Natal, Durban 4001, South Africa*, [7]*Physics Department, Durban University of Technology, Durban 4000, South Africa*, [8]*Science Institute, University of Iceland, 107 Reykjavík, Iceland*, [9]*CNR-IMM, Unit of Agrate Brianza, Via C. Olivetti 2, Agrate Brianza 20864, Italy*, [10]*Institute for Materials Science and Center for Nanointegration Duisburg-Essen (CENIDE), University of Duisburg-Essen, 45141 Essen, Germany*, [11]*School of Particles and Accelerators, Institute for Research in Fundamental Sciences (IPM), P.O. Box 19395-5531, Tehran, Iran.*

Spokesperson: [Hilary Masenda] [hilary.masenda@wits.ac.za]
Contact person: [Juliana Schell] [juliana.schell@cern.ch]

CERN-INTC-2024-018 / INTC-P-697
10/01/2024

Abstract

Halide perovskites have been at the centre of intense research over the past decade, as an emerging material class for potential optoelectronic applications with more emphasis on photovoltaics. Although halide perovskites have a high defect tolerance, an understanding of defects and dopants is vital for enhancing performance and extending the range of optoelectronic applications beyond solar cells. More precisely, knowledge of the chemical nature of dopants and defects is needed, coupled with the establishment of how crystal quality currently limits the efficiency. We propose optical and atomic scale characterization via hyperfine interactions using radiotracer photoluminescence (r-PL) and emission Mössbauer spectroscopy (eMS), respectively. ^{56}Mn* ($T_{1/2} = 2.6$ h) and ^{119}Sb* ($T_{1/2} = 38.2$ h) will be utilized for r-PL while the element-specific Mössbauer states will be populated via ^{57}Mn* ($T_{1/2} = 85.4$ s) and ^{119}In* ($T_{1/2} = 2.4$ min). The proposed experiments will be undertaken on both (a) inorganic and (b) hybrid inorganic-organic halide perovskites with (A = Cs^{+}, Rb^{+}, MA^{+}, or FA^{+}; B = Pb^{2+} or Sn^{2+}; X = Cl^{-}, Br^{-}, or I^{-}) that will be alloyed/mixed at any of the three different sites of the ABX_3 crystal structure. The presence of clearly defined features observed on a test emission Mössbauer spec-trum obtained from $(Cs_{0.15}FA_{0.85})Pb(I_{0.78}Br_{0.22})_3$ confirms that the implantation parameters used are sufficient to maintain the structure of the hybrid perovskite thin films, thus confirming the usefulness of the proposed experiments.

Requested shifts: [15] shifts, (split into [6-7] runs over [2] years)
Experimental Area: GLM and off-line lab (508-R-001)

1 Introduction and Motivation

Perovskites are a special class of compounds that have a crystal structure similar to calcium titanate ($CaTiO_3$)[1], with general chemical formula ABX_3, where "X" is an anion bonding with "A" and "B" cations with different sizes. Over the past two decades, halide perovskites[2,3] have attracted significant scientific interest mainly due to increased efficiency when applied in solar cells, competing with long-standing silicon-based photovoltaics. Si has been, and still is, the most widely used material in the photovoltaic industry[4]. This is evident from the number of research outputs over time, see Fig 1 (a). Recently, the number of indexed publications reporting the use of perovskites in solar cells has been dominating research outputs, as depicted in Fig 1 (b). Initially, perovskites were applied as a sensitizer in a dye solar cell in 2009[5] with power conversion efficiencies (PCE) ∼3.8%. Significant research spawned when PCE values of ∼10-11% were demonstrated in 2012[6,7]. In just over a decade, PCE values of single-junction perovskite-based solar cells have increased rapidly, with the current value standing at 26.1 %[8]. Morever, Si-perovskite tandem solar cells have already surpassed the Si fundamental limit; Fig 1 (c). A new record of 33.9% was recently set by LONGi Green Energy Technology Co Ltd[9].

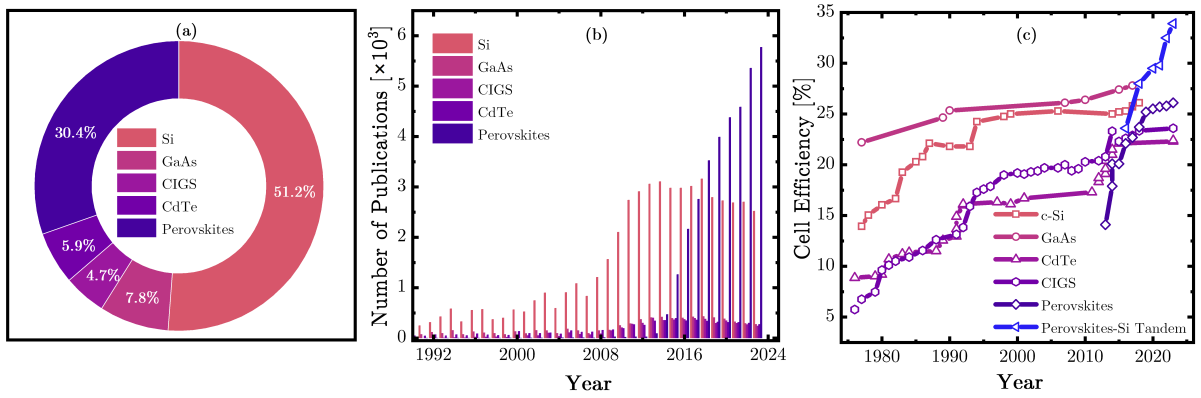

Figure 1: *Trends in indexed publications related to material systems used in photovoltaics (searched from Scopus using the related topic 'keyword' indicated extracted on 31.12.2023 limited to solar cells or photovoltaics). (a) Relative (%) outputs in different materials over time and (b) yearly progress in various key materials, while (c) shows the corresponding power conversion efficiencies adopted from NREL[9].*

Perovskite materials possess superior photoelectric properties such as direct band gap, strong light absorption, high luminous efficiency, strong carrier mobility, high ion conductivity, and long carrier lifetime[10–12]. These properties make halide perovskites candidates for potential applications in other optoelectronic devices beyond solar cells, such as lasers, light-emitting diodes and photodetectors[12–28]. This is supported by the increase in the number of publications over the past decade as shown in Fig 2; 35% coming from non-photovoltaic research outputs. Moreover, commonly known from III-V semiconductors[29,30], alloying offers the ability to tune material properties by varying the composition of constituent atoms to realize extended functionality. Similarly, halide perovskites can be alloyed on either A, B or X sites thereby tuning electronic and optical properties to target specific applications[28]. For instance, alloying on the X-site with halogens offers broadband wavelength tunability in the visible light region from ∼400 nm (Cl) to ∼700 nm (I) for $CsPbX_3$ perovskites[31]. However, I and Cl have a low propensity to mix

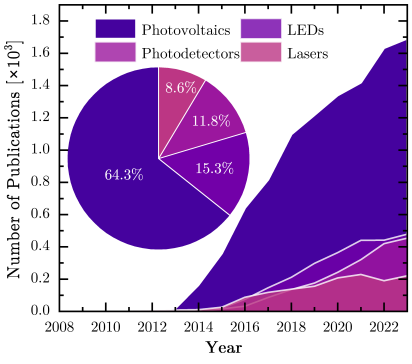

Figure 2: *Biased selection of indexed publications in Scopus on applications of halide perovskites. The inset shows percentage contributions over time until 31.12.2023.*

due to lattice mismatch stemming from the large atomic size difference. On the other hand, Im *et al*[32] demonstrated that the wavelength range can be extended into the near-infrared region (up ∼1100 nm) by using $MA(Pb_xSn_{1-x})I_3$. Finally, mixing on the A-site offers hybrid organic-inorganic halide perovskites. These display a relatively narrow wavelength range; ∼720 - 840 nm was reported for $(Cs_xFA_{1-x})PbI_3$[33].

A key component in realizing practical applications in devices is the thermodynamic stability of halide perovskites and their alloys. Over the years, the Goldschmidt tolerance (t) and octahedral factors (μ) have been used to predict known perovskite materials based on the stability and formability of the resulting ABX_3 crystal structure[34,35]. The factors are defined by the equations: $t = (r_A + r_X)/[\sqrt{2}(r_B + r_X)]$ and $\mu = r_B/r_X$ where r_A, r_B and r_X are radii for the ion at the corresponding site. Appropriate conditions for both factors are set by the inequalities; $0.813 < t < 1.107$ and $0.377 < \mu < 0.895$[34]. Moreover, alloyed materials are often associated with structural fluctuations[29,36] which may impede the desired or envisaged electronic, optical and/or magnetic properties. A deeper understanding of the disorder-induced effects is vital for prospective perovskite alloy-based devices since the presence of a disorder potential strongly affects the in-plane carrier transport properties[36–38].

Furthermore, transition metal ion doping in caesium lead halide perovskite nanocrystals has been demonstrated as an effective method to tune the optical properties for desired applications ranging from light-emitting diodes, solar cells and micro-lasers to photodetection[12,28]. Mn dopants in nanocrystals (NCs) based on halide perovskites have been demonstrated to enhance luminescence[39]. Meanwhile, some B-site ions, such as Mn doping, can lead to broad emission due to self-trapped excitons, which demonstrate the potential of applications in white-light applications[40,41].

In addition, there are several DFT reports[42–47] that have suggested the presence of spin-orbit coupling (SOC) in noncentrosymmetric hybrid organic-inorganic halide perovskites stemming from Rashba, Rashba/Dresselhaus, or Dresselhaus effects[48]. Currently, there are similar predictions in all-inorganic halide perovskites[49]. This presents opportunities for extending halide perovskites applications to spin-based devices.

Even though halide perovskites and their alloys and/or organic-inorganic hybrids have high defect tolerances, an understanding of defects and dopants is vital for enhancing performance and extending the range of optoelectronic applications. More precisely, the chemical nature of defects; shallow or deep, coupled with establishing whether crystal quality affects the current efficiency limits for different applications.

2 Aims and objectives

The main thrust of the project is to contribute to current research on perovskites which display new functional properties envisaged for a wide range of optoelectronic applications. The project will focus on both (a) inorganic and (b) hybrid inorganic-organic halide perovskites with (A = Cs^+, Rb^+; B = Pb^{2+} or Sn^{2+}; X = Cl^-, Br^-, or I^-). A suite of techniques will be utilized to investigate structural and optical properties. A wide range of structural characterization techniques, both laboratory- and synchrotron-based, will be utilized before and after the proposed experiments at ISOLDE. Subsequently, optical and atomic scale characterization via hyperfine interactions will be undertaken using radiotracer photoluminescence (r-PL) and

emission Mössbauer spectroscopy (eMS), respectively. On a fundamental level, a clear and full understanding of the mechanism by which charge carriers or energy is transferred and knowledge of the location and charge state of dopants and associated defects are of great importance in order to be able to control or tune photo-responsivity in these materials. The project will be guided by the following specific objectives:

(a) Determine the lattice sites, charge states of dopants (the daughter following decay) and the effect of implantation-induced damage (and related annealing behavior) through hyperfine interactions and their temperature dependence.

(b) Explore the influence of alloy concentration (x) on different lattice sites and dopants using hyperfine parameters to establish any correlation with the Goldschmidt tolerance and octahedral factors.

(c) Linked with (a) and (b), establish the role or influence of different dopants and alloy combinations on the band structure and excitonic features; specifically, how these influence optical and electronic properties.

(d) Investigate the influence of laser excitation on the local environment surrounding the probe element and correlate with luminescence features observed under equivalent experimental conditions of laser excitation energy, laser power and sample temperature.

(e) Ascertain the influence of alloy/implantation-induced disorder on the excitonic features in doped and alloyed perovskites from temperature-dependent PL measurements.

(f) Study the charge-transfer and energy-transfer properties of doped and/or halide perovskites to establish suitable optoelectronic applications.

3 Materials, Methods and Proposed Experiments

3.1 Halide Perovskites

Metal halide perovskites can be deposited with a variety of methods resulting in different morphologies and defect densities. Thanks to the extensive laboratory infrastructure at Fraunhofer ISE and the University of Freiburg we will be able to fabricate samples of both organic and inorganic thin films using vacuum-based and solution-based deposition techniques. In the vacuum-based approaches the precursors are heated in thermal sources inside of a vacuum chamber. As the vapours rise, they condense on the substrate and a uniform, conformal perovskite thin-film forms. When depositing from the solution, all precursors are dissolved and the resulting solution is spread on a substrate (for example via spin-coating) to form a layer.

Several halide perovskite samples will be synthesized and studied covering;

(a) inorganic alloyed both on (i) the halide (X) site $AB(X_xX'_{x-1})_3$ where A:Cs, B: Pb, and X or X′: Cl, Br and I, (ii) the divalent (B) site $A(B_xB'_{x-1})X_3$ where A:Cs, B or B′: Pb, Sn or Ge and X: Cl, Br or I and finally

(b) hybrid organic-inorganic systems which are alloyed on the monovalent cation or A site,$(A_xA'_{x-1})BX_3$ where A: Cs or A′: formamidinium (denoted FA, with the composition CH_5N_2) or methyl-ammonium (denoted MA, with the composition CH_6N),B′: Pb and X: Cl, Br or I.

Different inorganic and hybrid organic-inorganic halide perovskites will be prepared to target concentration (x) with values: 0, 0.3, 0.5, 0.7 and 1.

3.2 Emission Mössbauer Spectroscopy

Emission Mössbauer spectroscopy has been used at ISOLDE for several decades to study dopants' lattice sites, charge and spin states, binding properties, magnetic interactions and dynamic effects such as paramagnetic relaxations. Over the years experiments predominantly have been applied to semiconductors such as II-VI oxides, ternary III-nitrides, and halides mainly using ^{57}Mn* ($T_{1/2}$ = 85.4s) and ^{119}In* ($T_{1/2}$ = 2.4 min)[50–53]. The spectrum for $(Cs_{0.15}FA_{0.85})Pb(I_{0.78}Br_{0.22})_3$ obtained from a test eMS measurement on hybrid organic-inorganic halide perovskite is shown in Fig 3. Preliminary analysis of the required four spectral components with isomer shift values of D1: 0.61 mm/s, D2: 0.51 mm/s, D3: 0.77 mm/s and S1: -0.09 mm/s. The isomer shift values of 1.48, 1.13 and 0.78 mm/s are expected for dilute high-spin Fe^{2+} on the B site for Pb-X; for X: Cl, Br and I, respectively. These are estimated using a semi-empirical model developed by Gunnlaugsson and Masenda[54] from 22 compounds with δ values showing a standard deviation of $\pm$0.1 mm/s. The model considers nearest neighbour distances and electronegativity of the hosts and allows the assignment of this component to substitutional Fe^{2+}. The isomer shift for D3 is comparable to the Pb-I system, which is expected since the hybrid perovskite material is iodine-rich. However, there are no clear assignments for the remaining three spectral components. On a positive note, the presence of clearly defined features on the spectrum confirms that the implantation parameters employed are sufficient to keep the structure of the materials. This forms the basis for the experiments proposed herein; to unravel the missing gaps. A fundamental understanding of the different assignments forms the basis of the proposed prospective experiments starting with simple halide systems and then alloyed on a single site, i.e. either A, B or X. The use of short-lived radioactive isotopes implanted in materials and Mössbauer spectroscopy presents a unique two-fold approach; (i) material modification by introducing the desired (daughter) dopant and (ii) characterization at the atomic scale of the local environment of the probe nucleus via the decay products (i.e. γ-rays). The following experiments are planned:

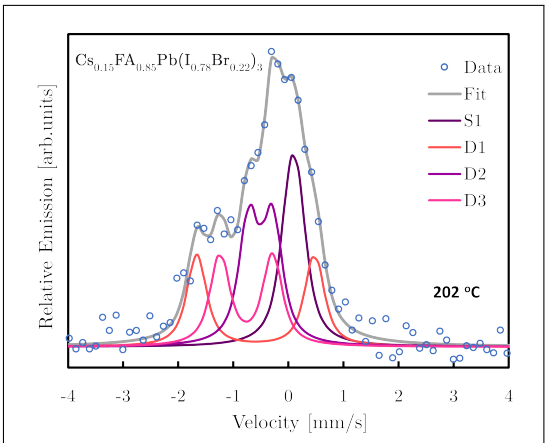

Figure 3: ^{57}*Fe emission Mössbauer spectra obtained at emission angle of 60^o with the sample held 480 K*

(M1) ^{57}Mn*: Series of temperature-dependent measurements, where samples are measured at low and high temperatures. The results give the first indications of the annealing profile of the implantation-induced damage (less intensity at increasing temperatures). The temperature dependence will also inform the stability of different halide perovskites at high temperatures.

(M2) ^{119}In*: For specific compositions, the use ^{119}In* implantations for ^{119}Sn eMS will offer a suitable option for doping the B-site for temperature-dependent measurements. This will give new information on the annealing of implantation damage, and knowledge concerning In-defect complexes and their stability. Moreover, toxicity due to lead is an outstanding issue in halide perovskites. Several attempts have been made to replace Pb with Sn, however, Sn^{2+} usually oxidizes to Sn^{4+}. The use of ^{119}In* will inform on the preferred lattice site, charge states and impact on optoelectronic properties. An understanding of the oxidation mechanism is crucial for the use of Sn in lead-free solar cells.

(M3) Online laser excitation; the new eMIL set-up allows for laser excitation while undertaking online eMS using both isotopes. This approach will offer insights on the influence of laser excitation on hyperfine parameters which will be correlated to optical properties obtained from r-PL under equivalent conditions.

3.3 Radiotracer Photoluminescence

Photoluminescence (PL) is a widely used technique for semiconductor characterization. PL is mainly used to determine the optical band gap of semiconducting materials. The principle behind PL explores laser excitation (typically energy higher than the bandgap of the material under study) which illuminates the semiconductor. This excites transitions within the material which recombine within the crystal, sometimes at impurity sites as bound excitons if the semiconductor is extrinsically doped with impurities or recombine at structural defect sites or intrinsic defects. This recombination is analyzed using a spectrometer and from this, an optical spectrum characteristic of the semiconductor is produced. In addition to band gap determination, PL will provide information on electronic defects, local disorder, phase distribution, photo-induced halide segregation and material degradation of the halide perovskites[55,56]. Moreover, the application of radioactive isotopes to traditional PL is a very clear way to remove chemical blindness. Observing the appearance and disappearance of spectral features stemming from decay products related to introduced radioactive isotopes allows for unequivocal chemical identification of elemental species in the material[57]. Samples will be implanted at GLM in the SSP chamber using ^{56}Mn* ($T_{1/2}$ = 2.58 hrs) and ^{119}Sb* ($T_{1/2}$ = 38.19 hrs). This will be subsequently followed by PL measurement in an offline laboratory (508-R-001) at ISOLDE to undertake the following experiments:

(P1) Temperature-dependent measurements. The variation of PL peak energies and spectral linewidths with temperature provides a measure of the presence or absence of a disorder potential in a materials systems. This disorder could be due to statistical fluctuations in the spatial distribution of alloying elements and/or implantation-induced defects.

(P2) Power series measurements at low and room temperatures to ascertain the effect of excitation power on the excitonic features leading to the assignment of their identity. The PL intensity (I_{PL}) depends on the laser excitation power (P) related by the expression, $I_{PL} \propto P^{\alpha}$[58], where α is a representative of the radiative recombination mechanism.

(P3) Circularly polarized (right- or left-handed) excitation to investigate any SOC-induced splitting at the conduction band or valence band. The results would offer insight for further studies.

3.4 Structural Characterization

X-ray diffraction and Scanning Electron Microscopy measurements are commonly used to characterize metal halide perovskite films. These offer a fast way to check the quality of thin films intended for integration into optoelectronic devices. They do leave many questions open for which more in-depth characterization like the ones proposed here are needed. Moreover, synchrotron-based X-ray techniques such as X-ray diffraction (XRD), X-ray fluorescence (XRF), X-ray photoelectron spectroscopy (XPS), X-ray Absorption Near Edge Spectroscopy (XANES), X-ray absorption fine-structure (XAFS), coherent diffraction imaging (CDI), Bragg CDI and ptychography will be utilized. Synchrotron X-ray sources are superior to laboratory-based ones as they offer a more coherent X-ray beam with high flux and brightness, broad wavelength

range, and tuneable energy. As a result, synchrotron-based X-ray techniques allow for improved phase identification and refined crystal structural information. We will determine the materials' structure, composition, and strain coupled with the ability to view the morphology in 3D among other materials properties using these techniques. Furthermore, at synchrotron facilities, there are possibilities for performing in-situ measurements, building unique set-ups and the availability of specialized instrumentation such as high-performance detectors that will aid our investigations.

3.5 Simulations/Theory

Ab initio calculations within the context of density functional theory (DFT) like Quantum-ESPRESSO[59], SIESTA[60], VASP[61] and/or Wien2k[62] are also proposed to support the research activities described herein. DFT is a well-established method for first principles band structure calculations and has been successfully applied to solid-state systems including halide perovskites. These calculations will include determinations of band gaps, absolute band-edge positions, effective mass, formation energy and hyperfine interaction parameters including isomer shift and quadrupole splitting to support experimental observations.

4 Beam request/Isotopes

Experiments are planned to target 6-7 beam-times split between eMS and PL measurements over 2 years; 2-3 beam times per year spread between the two major techniques will allow for the completion of the proposed studies. The table below gives the requested isotopes, planned experiments and time required.

Experiment	Isotope	Time (hrs)	Rationale
M1, M3	^{57}Mn*	60	$\sim$ 15-20 samples alloyed on different sites, 3 hrs/sample.
M2,	^{119}In*	20	a few selected alloys ($\sim$ 12 samples), 2 hrs/sample.
P1-P3	^{56}Mn*	8	$\sim$ 15-20 samples, collections at SSP and measure offline
P1-P3	^{119}Sb*	10	$\sim$ 15-20 samples, collections at SSP and measure offline
Calibration	^{57}Mn*, ^{119}In*,	19	$\sim$ 20 % based on past experience
Contingency	^{57}Mn*, ^{119}In*,	19	$\sim$ 20 % for exploring new phenomena in detail

Temperature series measures will require about 4-5 low-temperature steps and 3-4 high-temperature steps up to about 250° C for eMS measurements per sample.

5 Conclusions/Outlook

Halide perovskites possess fascinating properties which offer many potential practical applications in optoelectronic devices. Although they have been studied extensively over the past decades and are an established building block for photovoltaic materials, there are still many open questions to unravel on fundamental electronic and optical properties. The proposed study seeks to establish valuable information on defects, the lattice sites, charge (and spin) states of dopants and how these correlate to their observed optical or optoelectronic properties. Moreover, the proposed study will endeavour to explore a deeper understanding of the physics that underpins the peculiar functionalities of halide perovskite materials in not only enhancing photovoltaic properties but also applying the acquired knowledge in LEDs, lasers, photodetectors and possibly spintronics.

Summary of requested shifts:

Isotope	$T_{1/2}$	Intensity (Ions/μC)	Activity (MBq)	eMS	PL	Shifts requested
^{56}Mn*	2.6 h	4×10^8	29.6	N	Y	1.5
^{57}Mn*	85.4 s	$(2-3) \times 10^8$	online	Y	N	8
^{119}Sn*	2.4 min	$(2-3) \times 10^8$	online	Y	N	4
^{119}Sb*	38.2 h	5×10^7	2.50	N	Y	1.5
					Total	**15**

Ion Sources: **RILIS**, Beam Energy: $\geq$ **50 keV**, Target: **UC**$_x$

References

[1] R. J. Tilley, *Perovskites: structure-property relationships* (John Wiley & Sons, 2016).

[2] T.-C. Sum and N. Mathews, *Halide perovskites: photovoltaics, light emitting devices, and beyond* (John Wiley & Sons, 2019).

[3] W. Nie and K. K. Iniewski, *Metal-Halide Perovskite Semiconductors: From Physical Properties to Opto-electronic Devices and X-ray Sensors* (Springer Nature, 2023).

[4] S. Philipps and W. Warmuth, Photovoltaics Report (2023).

[5] A. Kojima, *et al.*, Journal of the American Chemical Society, **131**, 6050 (2009).

[6] M. M. Lee, *et al.*, Science, **338**, 643 (2012).

[7] H. S. Kim, *et al.*, Scientific Reports 2012 2:1, **2**, 1 (2012).

[8] M. A. Green, *et al.*, Progress in Photovoltaics: Research and Applications, **32**, 3 (2024).

[9] "Nrel best research-cell efficiency chart," `https://www.nrel.gov/pv/cell-efficiency.html`, accessed: 2023-12-27.

[10] G. M. Wilson, *et al.*, Journal of Physics D: Applied Physics, **53**, 493001 (2020).

[11] X. Liu, *et al.*, Nanotechnology Reviews, **11**, 3063 (2022).

[12] L. Zhang, *et al.*, Nano-Micro Letters, **15**, 177 (2023).

[13] A. Sadhanala, *et al.*, Nano Letters, **15**, 6095 (2015).

[14] S. D. Stranks and H. J. Snaith, Nature Nanotechnology, **10**, 391 (2015).

[15] T. Chiba, *et al.*, Nature Photonics 2018 12:11, **12**, 681 (2018).

[16] L. H. Zeng, *et al.*, Advanced Science, **6**, 1901134 (2019).

[17] S. D. Stranks, *et al.*, Advanced Materials, **31** (2019).

[18] G. Kakavelakis, *et al.*, Advanced Science, **7**, 2002098 (2020).

[19] C. Huang, *et al.*, Science, **367**, 1018 (2020).

[20] C. Qin, *et al.*, Nature 2020 585:7823, **585**, 53 (2020).

[21] Y. He, *et al.*, Nature Photonics 2021 16:1, **16**, 14 (2021).

[22] S. Deumel, *et al.*, Nature Electronics 2021 4:9, **4**, 681 (2021).

[23] X. Zhan, *et al.*, ACS Applied Materials and Interfaces, **13**, 45744 (2021).

[24] L. Zhang, *et al.*, Light: Science Applications 2021 10:1, **10**, 1 (2021).

[25] L. Zhu, *et al.*, Nature Communications 2021 12:1, **12**, 1 (2021).

[26] Z. Liu, *et al.*, Advanced Materials, **33**, 2103268 (2021).

[27] J. S. Kim, *et al.*, Nature 2022 611:7937, **611**, 688 (2022).

[28] Q. Wei, *et al.*, Advanced Photonics Research, **4**, 2200236 (2023).

[29] S. Adachi, *Properties of Semiconductor Alloys: Group-IV, III-V and II-VI Semiconductors* (John Wiley & Sons, Ltd, Chichester, UK, 2009) ISBN 9780470744383, pp. 1–400.

[30] S. Nakamura, Rev. Mod. Phys., **87**, 1139 (2015).

[31] L. Protesescu, *et al.*, Nano Letters, **15**, 3692 (2015).

[32] J. Im, *et al.*, Journal of Physical Chemistry Letters, **6**, 3503 (2015).

[33] G. E. Eperon, *et al.*, Energy Environmental Science, **7**, 982 (2014).

[34] Q. Sun and W. J. Yin, Journal of the American Chemical Society, **139**, 14905 (2017).

[35] Q. A. Akkerman and L. Manna, ACS Energy Letters, 604 (2020).

[36] C. Weisbuch, *et al.*, Nanophotonics, **10**, 3 (2021).

[37] H. Masenda, *et al.*, Advanced Electronic Materials, **7**, 2100196 (2021).

[38] S. D. Baranovskii, *et al.*, ACS Omega, **0** (2022).

[39] S. Feldmann, *et al.*, Journal of the American Chemical Society, **143**, 8647 (2021).

[40] S. Feldmann, *et al.*, Advanced Optical Materials, 2100635 (2021).

[41] J. Hao and X. Xiao, Frontiers in Chemistry, **9**, 822106 (2022).

[42] F. Brivio, *et al.*, Physical Review B - Condensed Matter and Materials Physics, **89**, 155204 (2014).

[43] M. Kim, *et al.*, Proceedings of the National Academy of Sciences of the United States of America, **111**, 6900 (2014).

[44] A. Stroppa, *et al.*, Nature Communications 2014 5:1, **5**, 1 (2014).

[45] J. Even, *et al.*, physica status solidi (RRL) – Rapid Research Letters, **8**, 31 (2014).

[46] M. Kepenekian, *et al.*, ACS Nano, **9**, 11557 (2015).

[47] W. Sukmas, *et al.*, Journal of Physical Chemistry C, **123**, 16508 (2019).

[48] J. S. Manser, *et al.*, Chem. Rev., **116**, 12956 (2016).

[49] P. R. Anandan, *et al.*, Applied Physics Reviews, **10**, 41312 (2023).

[50] H. P. Gunnlaugsson, *et al.*, Applied Physics Letters, **97**, 142501 (2010).

[51] R. Mantovan, *et al.*, Advanced Electronic Materials, **1**, 1400039 (2015).

[52] H. Masenda, *et al.*, New J. Phys, **24**, 103007 (2022).

[53] H. P. Gunnlaugsson, *et al.*, Physical Review B, **106**, 174108.

[54] H. P. Gunnlaugsson and H. Masenda, Journal of Physics and Chemistry of Solids, **129**, 151 (2019).

[55] T. Kirchartz, *et al.*, Advanced Energy Materials, **10**, 1904134 (2020).

[56] T. P. A. V. D. Pol, *et al.*, Advanced Optical Materials, **10**, 2102557 (2022).

[57] K. Johnston, *et al.*, Journal of Physics G: Nuclear and Particle Physics, **44**, 104001 (2017).

[58] T. Schmidt, *et al.*, Physical Review B, **45**, 8989 (1992).

[59] P. Giannozzi, *et al.*, Journal of Physics Condensed Matter, **21**, 395502 (2009).

[60] E. Artacho, *et al.*, Journal of Physics Condensed Matter, **20**, 6 (2008).

[61] J. Hafner, Journal of Computational Chemistry, **29**, 2044 (2008).

[62] P. Blaha, *et al.*, Journal of Chemical Physics, **152**, 74101 (2020).

6 Details for the Technical Advisory Committee

6.1 General information

Describe the setup which will be used for the measurement. If necessary, copy the list for each setup used.

- ☒ Permanent ISOLDE setup: *GLM beamline*
  - ☒ To be used without any modification
  - ☐ To be modified: *Short description of required modifications.*
- ☐ Travelling setup (*Contact the ISOLDE physics coordinator with details.*)
  - ☒ Existing setup, used previously at ISOLDE: *Emission Moessbauer Spectrometer from Ilmenau (eMIL).*
  - ☐ Existing setup, not yet used at ISOLDE: *Short description*
  - ☐ New setup: *Short description*
- ☒ Permanent ISOLDE setup: *SSP Photoluminescence Spectrometer*
  - ☒ To be used without any modification
  - ☐ To be modified: *Short description of required modifications.*

6.2 Beam production

For any inquiries related to this matter, reach out to the target team and/or RILIS (please do not wait until the last minute!). For Letters of Intent focusing on element (or isotope) specific beam development, this section can be filled in more loosely.

- Requested beams:

Isotope	Production yield in focal point of the separator ($/\mu$C)	Minimum required rate at experiment (pps)	$t_{1/2}$
^{57}Mn*	4×10^8	$< 10^9$ s^{-1}	85.4 s
^{119}In*	$2 - 3 \times 10^8$	$< 10^9$ s^{-1}	2.4 min
^{56}Mn*	$2 - 3 \times 10^8$	$< 10^9$ s^{-1}	2.6 h
^{119}Sb*	4×10^7	$< 10^9$ s^{-1}	38.2 h

- Full reference of yield information (*yield database for ^{57}Mn* and IS630 for ^{119}In**)
- Target - ion source combination:UC_x
- RILIS? (*Yes for all elements*)
  - ☐ Special requirements: (*isomer selectivity, LIST, PI-LIST, laser scanning, laser shutter access, etc.*)
- Additional features?
  - ☒ Neutron converter: (*for isotopes 1, 2 but not for isotope 3.*)
  - ☐ Other: (*quartz transfer line, gas leak for molecular beams, prototype target, etc.*)
- Expected contaminants: *Isotopes and yields*
- Acceptable level of contaminants: (*By using RILIS, no significant contaminants are expected*)
- Can the experiment accept molecular beams? *No*
- Are there any potential synergies (same element/isotope) with other proposals and LOIs that you are aware of? *IS630, IS681, IS683, IS670*

6.3 HIE-ISOLDE

For any inquiries related to this matter, reach out to the ISOLDE machine supervisors (please do not wait until the last minute!).

- HIE ISOLDE Energy: *(MeV/u); (exact energy or acceptable energy range)*
  - ☒ Precise energy determination required
  - ☐ Requires stable beam from REX-EBIS for calibration/setup? *Isotope?*
- REX-EBIS timing
  - ☒ Slow extraction
  - ☐ Other timing requests
- Which beam diagnostics are available in the setup?
- What is the vacuum level achievable in your setup?

6.4 Shift breakdown

The beam request only includes the shifts requiring radioactive beam, but, for practical purposes, an overview of all the shifts is requested here. Don't forget to include:

- Isotopes/isomers for which the yield need to be determined
- Shifts requiring stable beam (indicate which isotopes, if important) for setup, calibration, etc. Also include if stable beam from the REX-EBIS is required.

An example can be found below, please adapt to your needs. Copy the table if the beam time request is split over several runs.

Summary of requested shifts:

With protons	Requested shifts
Yield measurement of isotope 1	Included data taking
Optimization of experimental setup using isotope 2	Included data taking
Data taking, ^{57}Mn*	8.0
Data taking, ^{119}In*	4.0
Data taking, ^{56}Mn*	1.5
Data taking, ^{119}Sb*	1.5
Without protons	Requested shifts
Stable beam from REX-EBIS (after run)	Done with IS630
Background measurement	

6.5 Health, Safety and Environmental aspects

6.5.1 Radiation Protection

- If radioactive sources are required:
  - Purpose? *Online experiment with ^{57}Mn* and ^{119}In**
  - Isotopic composition? *^{57}Mn* and ^{119}In**
  - Activity? *300 MBq online with no manipulation. Manipulation with only 30 kBq according to the existing and approved procedure.*
  - Sealed/unsealed? *Unsealed*
- For collections:

- Number of samples? *20 samples each for $^{56}Mn^*$ and $^{119}Sb^*$*
- Activity/atoms implanted per sample? *29.6 MBq for $^{56}Mn^*$ and 2.5 MBq for $^{119}Sb^*$*
- Post-collection activities? (*Measurements in the SSP Photoluminescence Set in b.508-R-001*)

6.5.2 Only for traveling setups

- Design and manufacturing
  - ☐ Consists of standard equipment supplied by a manufacturer
  - ☒ CERN/collaboration responsible for the design and/or manufacturing: *ISIEC file of eMIL can be found at EDMS: 1317710.*
- Describe the hazards generated by the experiment:

Domain	Hazards/Hazardous Activities		Description
Mechanical Safety	Pressure	☐	[pressure] [bar], [volume][l]
	Vacuum	☒	10^{-5} mbar
	Machine tools	☒	Alignment of eMIL with GLM
	Mechanical energy (moving parts)	☒	Stepping motor on 4-positions lid
	Hot/Cold surfaces	☒	Cold and hot lids
Cryogenic Safety	Cryogenic fluid	☒	LN_2 (4 liters/load)
Electrical Safety	Electrical equipment and installations	☒	see ISIEC file at EDMS: 1317710
	High Voltage equipment	☒	1000 V bias detector
Chemical Safety	CMR (carcinogens, mutagens and toxic to reproduction)	☐	[fluid], [quantity]
	Toxic/Irritant	☐	[fluid], [quantity]
	Corrosive	☐	[fluid], [quantity]
	Oxidizing	☐	[fluid], [quantity]
	Flammable/Potentially explosive atmospheres	☐	[fluid], [quantity]
	Dangerous for the environment	☐	[fluid], [quantity]
Non-ionizing radiation Safety	Laser	☒	HeCd, 325 nm, 50 mW, Class: 3B or
	Laser	☒	Compact 405 nm, 4.50 mW, Class: 2
	Magnetic field	☒	0.6 T (<0.1 out EMIL chamber)
Workplace	Excessive noise	☐	
	Working outside normal working hours	☒	As per ISOLDE schedule
	Working at height (climbing platforms, etc.)	☐	
	Outdoor activities	☐	
Fire Safety	Ignition sources	☐	
	Combustible Materials	☐	
	Hot Work (e.g. welding, grinding)	☐	
Other hazards	$^{57}Mn^*$ and $^{56}Mn^*$ are high-energy beta emitters		
	$^{119}In^*$: activity of the online experiment could be high and to be supervised by RP		